Rare Metal Materials and Engineering
Volume 51, Issue 9, September 2022
Available online at www.rmme.ac.cn

Science Press

Cite this article as: Yang Shengze, Cao Hui, Liu Yang, et al. Molecular Dynamics Simulation of Effect of Rough Surface on Material Removal and Subsurface Defects During γ-TiAl Machining[J]. Rare Metal Materials and Engineering, 2022, 51(09): 3236-3243.

ARTICLE

Molecular Dynamics Simulation of Effect of Rough Surface on Material Removal and Subsurface Defects During γ-TiAl Machining

Yang Shengze[1], Cao Hui[1,2], Liu Yang[1], Yao Peng[1], Feng Ruicheng[1,2]

[1] School of Mechanical and Electrical Engineering, Lanzhou University of Technology, Lanzhou 730050, China; [2] Key Laboratory of Digital Manufacturing Technology and Application, Ministry of Education, Lanzhou University of Technology, Lanzhou 730050, China

Abstract: The molecular dynamics method was used to simulate the machining response of nanoscale γ-TiAl. The rule-generated rough workpiece surface was used to study its effect on atom removal mechanism. The cutting process was investigated by varying the texture density and tool radius. Results show that the surface morphology of the workpiece has a non-ignorable influence on the generation of subsurface defects and the atom removal: the rough surface in the shear mode affects the generation of laminar fault shear zone. The increase in texture density increases the number of subsurface defects, and the integrity of the machined surface is different corresponding to different cutting patterns. The relative tool sharpness has an effect on the cutting mechanism and texture effects.

Key words: rough surface; atom removal; subsurface defects; molecular dynamics; γ-TiAl

In recent years, due to the popularity of the micro-electro-mechanical systems and the improvement of precision requirements, the micron- or nanometer-precision material processing has been widely used in aerospace field, automotive manufacturing, biomedical field, and optic/chip field[1-3], among which the defect generation and material quality should be taken into consideration. Zhang et al[4] studied the generation mechanism of surface defects of microscale Cu alloys and obtained the optimal reference cutting parameters. Golshan et al[5] investigated the influence of cutting parameters (cutting depth, feed rate, and cutting speed) on the surface quality of silicon during milling.

Due to its high strength, low density, and excellent high temperature performance, γ-TiAl alloy attracts much attention[6]. However, the generation of defects, such as cracks or phase transition, is inevitable in the machining process due to the room temperature brittleness of γ-TiAl alloy[7]. Priarone et al[8] studied the effects of tool parameters and tool coating on the cutting quality of γ-TiAl alloy, and found that the machinability of TiAl alloy can be improved by changing tool parameters and adding tool layers. He et al[9] discussed the characteristics of chip formation during the machining of Ti2AlNb alloy, and found that the chip morphologies and chip formation are greatly affected by the dynamic flow stress. Wang et al[10] analyzed the surface integrity of γ-TiAl alloys in the electrochemical machining process (ECM), and proved that ECM has no influence on the machined surface. However, few researches discuss the material processing at nanometer- or subnanometer-scale due to the high cost. Molecular dynamics (MD) is a common investigation method to study the mechanism of defect creation and material removal with a certain accuracy.

Similar to peridynamics, MD is a simulation method based on nonlocal theory[11]. Chamani et al[12] employed MD simulations to investigate the defect changes of Al/Ni multilayers during nano-indentation. Yasbolaghi et al[13] studied the crack propagation at the atomistic scale through MD function. Kazanc et al[14] used MD method to investigate

Received date: August 31, 2021
Foundation item: National Natural Science Foundation of China (52065036); Natural Science Foundation of Gansu (20JR5RA448); Hongliu First-Class Disciplines Development Program of Lanzhou University of Technology
Corresponding author: Feng Ruicheng, Ph. D., Professor, School of Mechanical and Electrical Engineering, Lanzhou University of Technology, Lanzhou 730050, P. R. China, Tel: 0086-931-5135199, E-mail: postfeng@lut.edu.cn

the crystallization behavior of CuNi alloy during annealing and the simulation results showed accurate predictability. In conclusion, MD is widely used in chemistry, biology, and first principles studies[15-17].

In the nanofabrication field, MD is the main research method due to the restrictions of experiment conditions. Xiao et al[18] studied the critical ductile-brittleness conversion processing depth of SiC. Goel et al[19] revealed the influence of elliptical vibration-assisted machining (EVAM) on the workpiece and proved that EVAM can reduce tool wear and achieve better machining quality. However, few researches discuss the effect of rough surfaces, a non-negligible processing factor. Li et al[20] studied the effect of rough surface on single crystal copper processing and found that the machining parameters should be ameliorated according to the specific rough surface at nanoscale. Papanikolaou et al[21] created the rough machined surface based on Weierstrass-Mandelbrot function and investigated the effect of fractal roughness in the grinding process. It is found that the high roughness is beneficial to the heat dissipation.

The mechanical properties of γ -TiAl alloy and the machining process under ideal conditions have been revealed in Ref.[22,23]. However, in the actual process, the workpiece surface is definitely rough. Therefore, in this research, the single crystal γ-TiAl alloy was used as the research object and MD method was applied to investigate the influence of texture density and tool radius in the nano-cutting process. In addition, the surface morphology of the material after machining and the influence of the tool retraction were also studied. It is found that the material removal modes are different with different tool radii and the generation of shear band is affected by the rough surface to some extent. The surface morphology and subsurface defects of the workpiece were also significantly affected by the tool retraction.

1 Model and Methods

Fig. 1 shows the L10 face-centered tetragonal (fct) cell structure of γ-TiAl alloy[24] with lattice constants of $a_0=b_0=$ 0.400 50 nm and c_0=0.407 07 nm[25]. The lattice constants in this simulation were $a_0=b_0$=0.4001 nm and c_0=0.4181 nm.

The nano-cutting model of regular rough surface was used for accurate simulation, as shown in Fig. 2. The related parameters are listed in Table 1. The workpiece was divided into Newton layer, thermostatic layer, and boundary layer to avoid the result error caused by scale effect. Since the hardness of diamond tools is much greater than that of the workpiece, the tool was set as a rigid body. The workpiece length in x, y, and z directions was 40, 20, and 20 nm, respectively. It should be noted that the texture density (R_0:R_x) was used in this research to replace the roughness. The cutting depth h was also defined in Fig.2. Thus, the influence of rough surface, i.e., the influence of texture densities, on the cutting progress was studied.

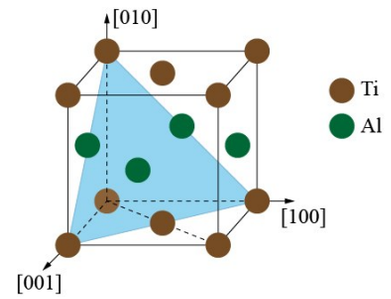

Fig.1 Schematic diagram of cell structure of γ-TiAl alloy

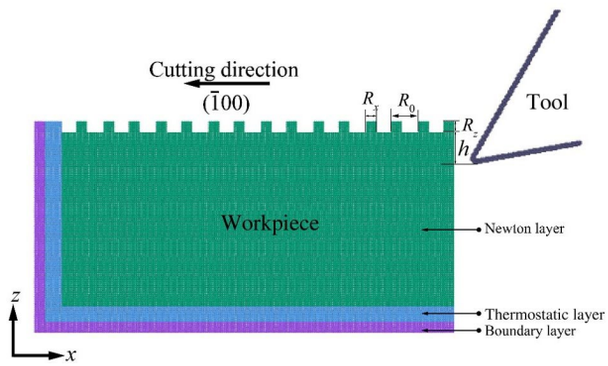

Fig.2 Schematic diagram of cutting model

Two kinds of tools were used for cutting experiments. Different relative sharpness of tool (RST) can produce different cutting modes, such as shearing and extrusion. In addition, RST can be obtained by the radio of the tool radius to the cutting depth. In this research, the texture density of workpiece was 0%, 20%, 40%, 60%, 80%, and 100%. The rough surface height R_z was 1 nm. The cutting direction of the

Table 1 Parameters of γ-TiAl workpiece and diamond tool

Parameter	γ-TiAl	Diamond tool
Dimension	40 nm×20 nm×20 nm	Radius of 0.5 and 8 nm
Cutting direction	[$\bar{1}$00] on (001)	-
Minimum texture width, R_0/nm	2.5	-
Minimum texture fill width, R_x/nm	0.0, 0.5, 1.0, 1.5, 2.0, 2.5	-
Texture height, R_z/nm	1	-
Rake angle/(°)	-	30, −10
Clearance angle/(°)	-	10
Tool thickness/nm	-	4

tool was [$\bar{1}$00], and the relative crystal face of the workpiece was (001).

For single-crystal γ-TiAl alloy, the potential functions, such as embedded-atom method (EAM)[26] and modified embedded-atom method (MEAM)[27] are commonly used. In this study, EAM potential function was used to describe the interaction between Ti and Al, as follows:

$$E = \sum_i F_i \left[\sum_{j(j \neq i)} f(r_{ij}) \right] + \frac{1}{2} \sum_{i,j(i \neq j)} \varphi_{ij}(r_{ij}) \quad (1)$$

where F_i is the embedded energy of atom i, φ_{ij} is the interaction energy between atom i and atom j, r_{ij} is the distance between atom i and atom j, and $f(r_{ij})$ is the host electron density at the site of atom i induced by other atoms in the system.

To reveal the tool force on the workpiece, the Morse potential function was used to describe the interaction between Ti-C and Al-C, as follows:

$$V(r) = D\left[1 - e^{-\alpha(r - r_0)/r_0}\right]^2 - D \quad (2)$$

where D is the interaction strength between two atoms, r_0 is the equilibrium distance between two atoms, r is the actual distance between two atoms, and α is the effective range. Thus, the interactions between Ti-C and Al-C can be obtained based on the data in Ref.[28], as shown in Table 2.

The large-scale atomic/molecular massively parallel simulator (LAMMPS) software[29] was used in this research. Table 3 shows the detail parameters of the simulation model. The tool trajectory is shown in Fig.3. Not only the machining response of the workpiece during cutting, but also the chip morphology after tool retraction was observed. After the simulation, OVITO software[30] was used to investigate the cutting model and the formation/evolution of defects. The common neighbor analysis (CNA) was applied to obtain the evolution law of lattice defects.

2 Results and Discussion

2.1 Cutting response at different texture densities in shear mode

To investigate the influence of texture density on cutting process, six texture densities were used. Fig. 4 shows the defect distributions at the cutting distance of 20 nm under different texture densities. Because RST is small, the traces of shear band can be clearly observed. Thus, with the tool radius of 0.5 nm, the cutting mode is shear mode. With increasing the texture density, the number of stacking faults is increased, and the average cutting depth is also increased, indicating that more slip systems are generated and ultimately leading to more multiple fault layers[22]. Obvious stacking slip bands can only be observed when the texture density is 0% or 100%, while the partial stacking slip bands and amorphous atoms can be observed when the texture density is between 0%~100%. This can be explained by the following reasons. The rough surface can disturb the stress waves induced by the tool. Thus, the complicated stress field in the shear zone results in easy interruption of the stacking fault growth. During the cutting process, the energy is mainly distributed in the chip formation and layer fault zones. The stacking shear band can reduce the energy in chip, i. e., the number of amorphous atoms in the chip is reduced, and the amorphous atoms have larger atomic kinetic energy than the ordered atoms do. The stress field in the chip formed by rough surface is complex and the stacking faults have the restriction effect. The regular sawtooth shape of chip can be observed in Fig. 4a and 4f, whereas the near sawtooth shape of chip is observed in Fig. 4b and 4e. The irregular chip can be observed in Fig. 4c and 4d. The more irregular the chip shape, the greater the energy in chip and the more the amorphous atoms. Hence, the workpiece does not have enough energy to form the shear band with a complete stacking fault. In addition, considering the effects of contact-induced amorphism (CIA) and strain-induced phase (SIP) transition[31], the rough surfaces lead to fluctuations in instantaneous cutting depth, resulting in chaotic stress states in CIA region, which hinders the growth in SIP region. It is inferred that these abovementioned reasons jointly lead to the formation of different cutting results.

Fig. 5 shows the defect distributions and machined surface morphologies after tool retraction and relaxation at texture density of 0%, 40%, 60%, and 100% with the cutting depth of 3 nm. Because most of the chip atoms stick to the tool and leave the workpiece when the tool retracts, only a small number of chip atoms form the burr by the stretching action. It is clear that in the shearing cutting mode, the effect of tool retraction on the subsurface is very little. However, the effect

Table 2 Morse potential function parameters between Ti-C and Al-C

Parameter	Interaction strength, D/eV	Effective range, α/nm^{-1}	Equilibrium distance between atoms, r_0/nm
Ti-C	0.982	22.83	0.1892
Al-C	0.280	27.80	0.2200

Table 3 Simulation model parameters of LAMMPS

Parameter	Value
Time step/fs	1
Simulation unit	Metal
Boundary condition	P P P
Simulation temperature/K	300
Equilibration step	50 000
Cutting distance/nm	20
Cutting speed/m·s^{-1}	100
Cutting depth/nm	3
Tool rising distance/nm	15

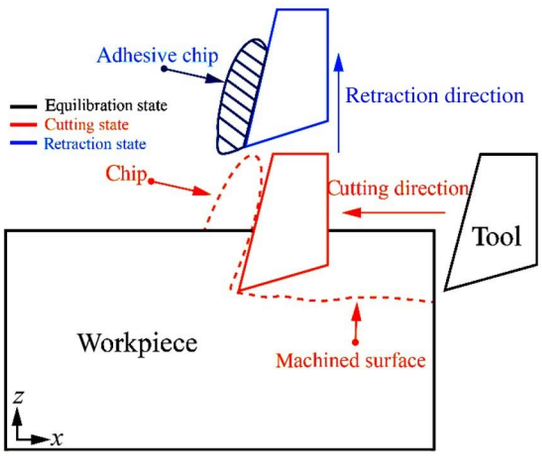

Fig.3 Schematic diagram of simulation model

degree is increased with increasing the texture density. The larger the texture density, the more the defect atoms on the machined surface. These defect atoms can be divided into two categories: defective atoms before tool retraction (DBTR) and defective atoms after tool retraction (DATR), as shown in Fig.5b. The number of DBTR is increased with increasing the average cutting depth, and the increase in the number of DATR is related to the stretching action. The larger the texture density, the higher the average cutting depth and the more the chip atoms. More force is required when the tool retracts, which results in tension stress on the left side and lower part of the tool. As a result, more defective atoms are generated with increasing the texture density. Accordingly, with increasing the texture density, more void defects are generated on the subsurface, and the quality of the processed surface is worse. Thus, the increase in texture density leads to inferior

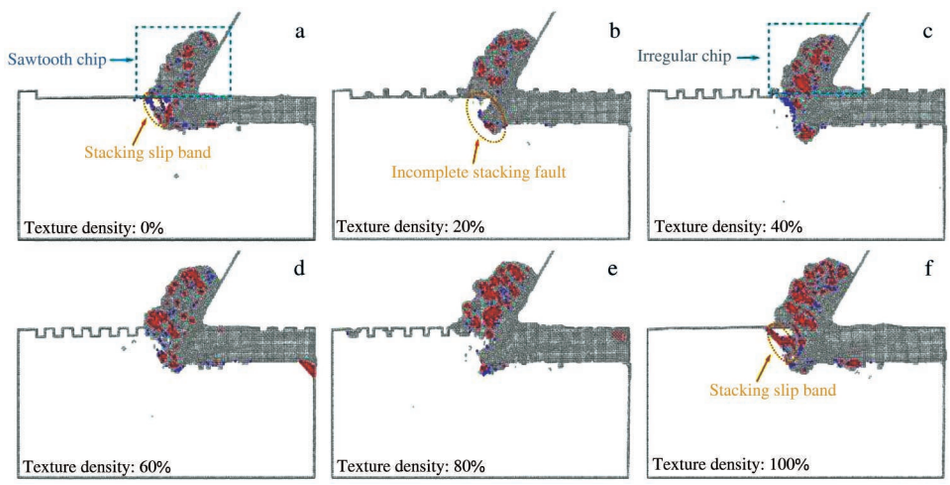

Fig.4 Defect distributions in shear mode at cutting distance of 20 nm and texture density of 0% (a), 20% (b), 40% (c), 60% (d), 80% (e), and 100% (f)

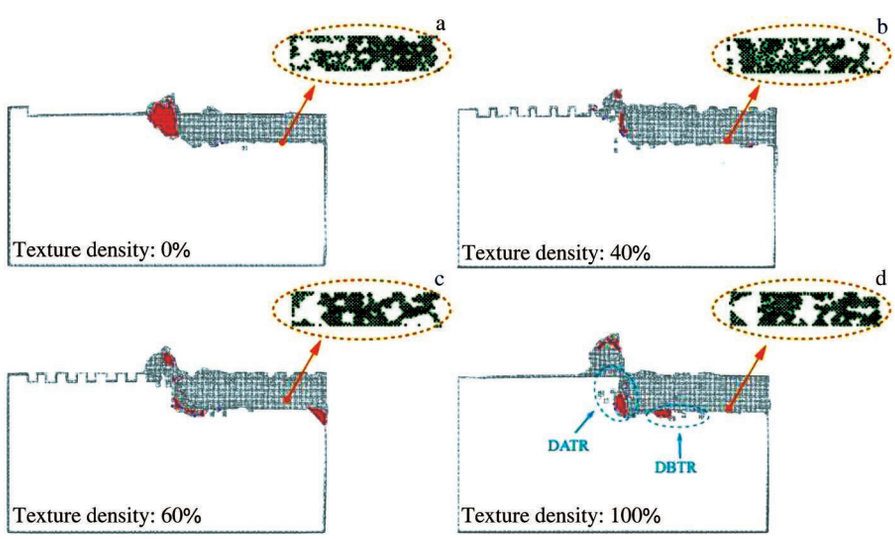

Fig.5 Defect distributions and machined surface morphologies after tool retraction and relaxation at texture density of 0% (a), 40% (b), 60% (c), and 100% (d)

surface integrity and more subsurface defects.

The surface morphology of the workpiece after machining is also very important. Fig.6 illustrates the height distributions of atoms on the workpiece surface at different texture densities. The burrs around the machining track can be observed, because of the flow accumulation of the atoms during cutting process. However, this factor is not sufficient enough to produce such a noticeable burr. The retraction process plays an important role in the burr formation: the tool atoms and the adhesive atoms on the tool have mutual attraction, resulting in tensile effect on the workpiece surface in retraction process. When the texture density is 0%, a small number of burrs are formed, as shown in Fig. 6a. With increasing the texture density, more burrs are formed due to the larger cutting depth. According to Fig. 6b, during cutting process, the rough surface around the tool path is nearly flat. After tool retraction, almost no burrs exist at the upper and lower ends of the tool. This is because the gaps on the rough surface can absorb atoms. Therefore, the rough surface can prevent further deterioration of machined surface quality. Particularly, the regular rough surfaces can reduce the production of sharp burrs at nanoscale.

Fig. 7 shows the cutting forces at different texture densities. As shown in Fig. 7a, the cutting force along x direction is obviously increased with increasing the texture density. The increase in the number of defective atoms and the enlargement of chip volume indicate the larger cutting force. However, along z direction, the cutting force at texture density of 100% is significantly lower than that of 0%. Other cutting force curves are inconstant because of the effect of rough surfaces on stress waves. Therefore, it can be clearly seen that with increasing the texture density, average F_z presents a downward trend, which is opposite to the trend of average F_x. This is due to the effect of large chip accumulation on the tool. The large amount of chip increases the radial force of the tool, while the opposite force of the workpiece on the tool is relatively small. Hence, the radial force is decreased, resulting in the reduction in average friction coefficients.

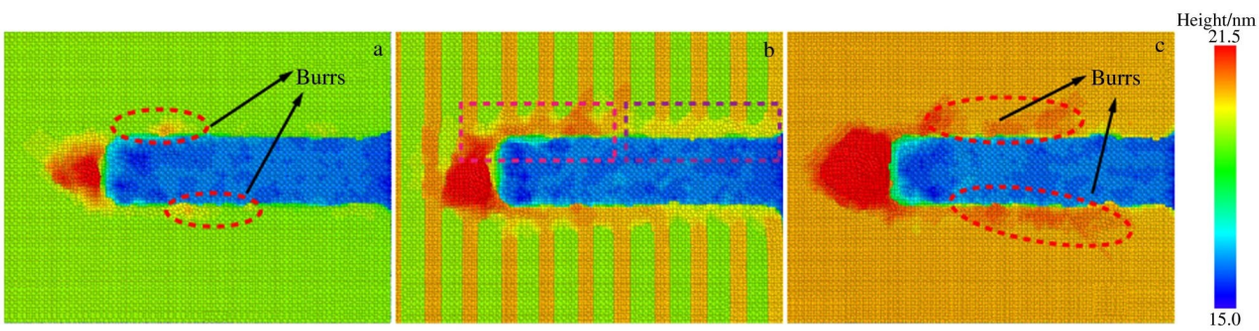

Fig.6 Height distributions of atoms on machined surfaces after tool retraction at texture density of 0% (a), 40% (b), and 100% (c)

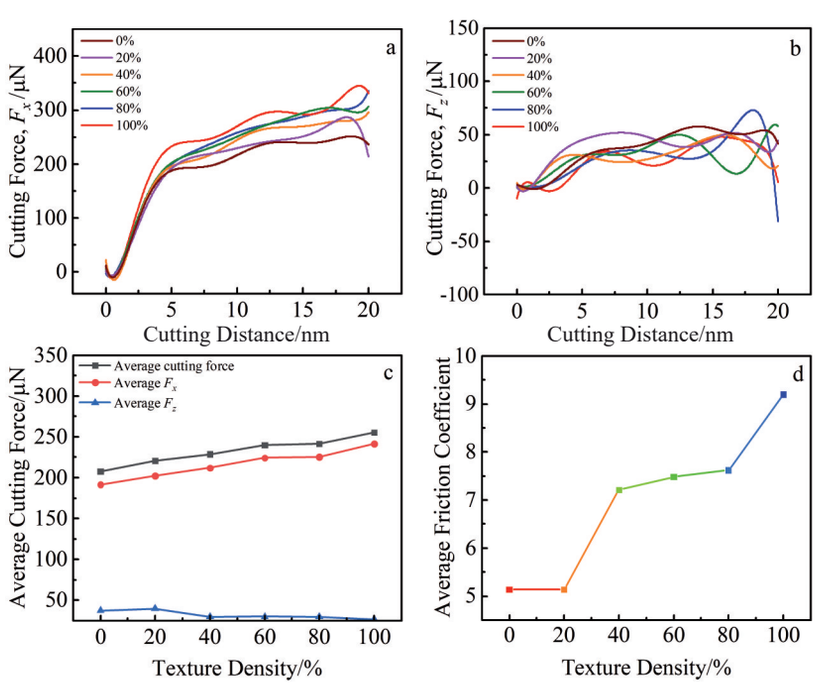

Fig.7 Cutting forces in shear mode along x direction (a) and z direction (b); average cutting forces (c) and average friction coefficients (d) at different texture densities

2.2 Cutting response at different texture densities in extrusion mode

When RST is greater than 1, the cutting mode is extrusion mode. Fig. 8 shows the defect distributions during cutting process at different texture densities with tool radius of 8 nm. Little chip appears in the cutting process due to the extrusion effect, resulting in more defects than the shear cutting process. In addition, with increasing the texture density, the stacking faults are smaller and denser. In the extrusion cutting process, the texture on the rough surface is pressed into the subsurface, resulting in a larger CIA region and then a disturbed subsurface stress field, which prevents the steady growth of faults.

Fig. 9 shows the surface morphologies, defect evolutions, and dislocation distributions during cutting process with texture density of 80%. The merging of textures is similar to the crack closure, as shown in Fig. 9a. Firstly, due to the extrusion effect of the tool, the workpiece subsurface in front of the tool produces a stacking fault with the $[10\bar{1}]$ plane. When the tool continues to move forward, the slip occurs to release the stress. However, the smooth slip cannot proceed along the $[10\bar{1}]$ direction due to the existence of other layer faults. The slip can only proceed along the $[\bar{1}01]$ direction. In addition, the dislocation slip and annihilation can be observed. Eventually, the slip of stacking faults connects two independent textures, which indicates that the extrusion can repair the surface cracks and internal cracks.

Fig. 10 shows the defect distributions and surface morphologies after cutting process in extrusion mode. After cutting process and relaxation, the workpiece with larger texture density produces more and bigger defects due to the full release of stress on the subsurface. The coupling effect reduces the defects in the front area of tool and increases the defects in the lower area of tool. During the stress release, the energy of small stacking faults is very high, resulting in the low stability and then the easy accumulation of large faults.

Unlike the shear cutting process, the extrusion cutting process produces less chip, and the chip becomes fluid across

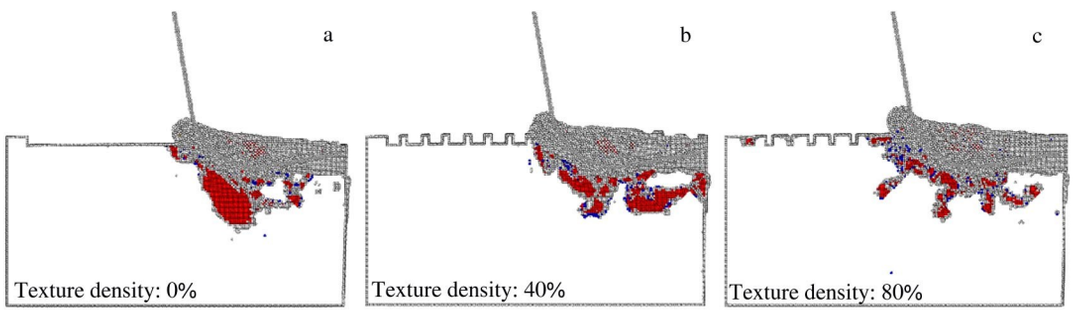

Fig.8 Defect distributions in extrusion mode at texture density of 0% (a), 40% (b), and 80% (c)

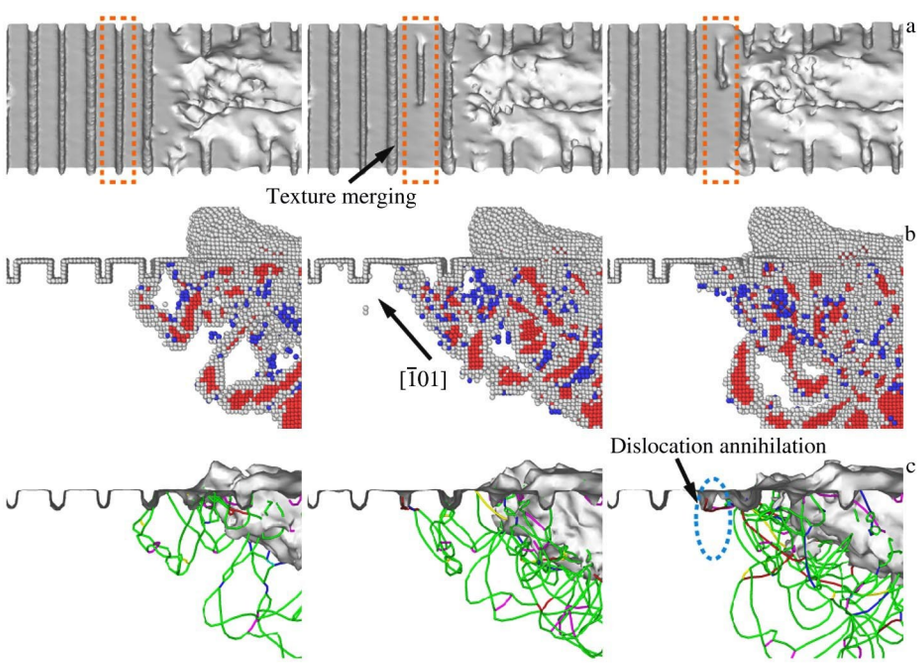

Fig.9 Surface morphologies (a), defect evolutions (b), and dislocation distributions (c) during extension cutting process with texture density of 80%

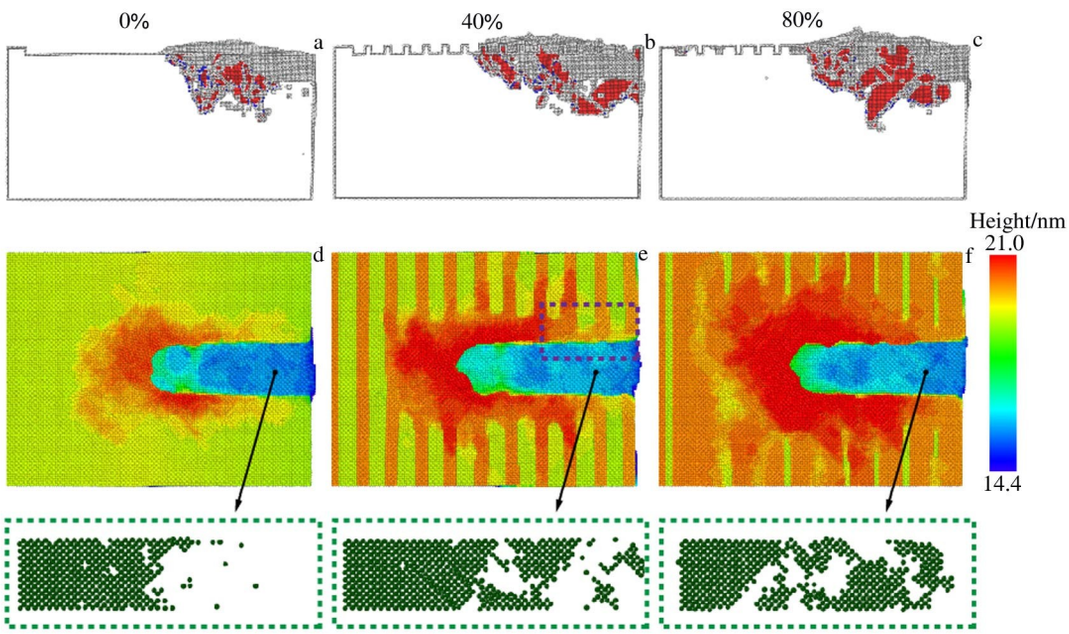

Fig.10 Defect distributions (a~c) and surface morphologies (d~f) after tool retraction and relaxation at texture density of 0% (a, d), 40% (b, e), and 80% (c, f)

the workpiece. Thus, the chip atoms are widely distributed. Fig. 10b shows a flattening phenomenon, which is similar to that in Fig. 6b. With increasing the texture density, the large stacking faults are easily generated and the processed surface becomes more chaotic. Meanwhile, the volume of the grooves in the workpiece becomes less and less, resulting in the fact that the chip is more widely distributed with increasing the texture density.

Fig. 11 shows the cutting forces and average friction coefficients with different texture densities in the extrusion cutting process. The cutting force in z direction in extrusion mode is much larger than that in shear mode. Both the shear force and radial force are increased with increasing the texture density, because the more the atoms pushed into the subsurface, the greater the radial force. The average cutting force and the average friction coefficient are increased with increasing the texture density, which is in a good agreement with the results in Ref.[20].

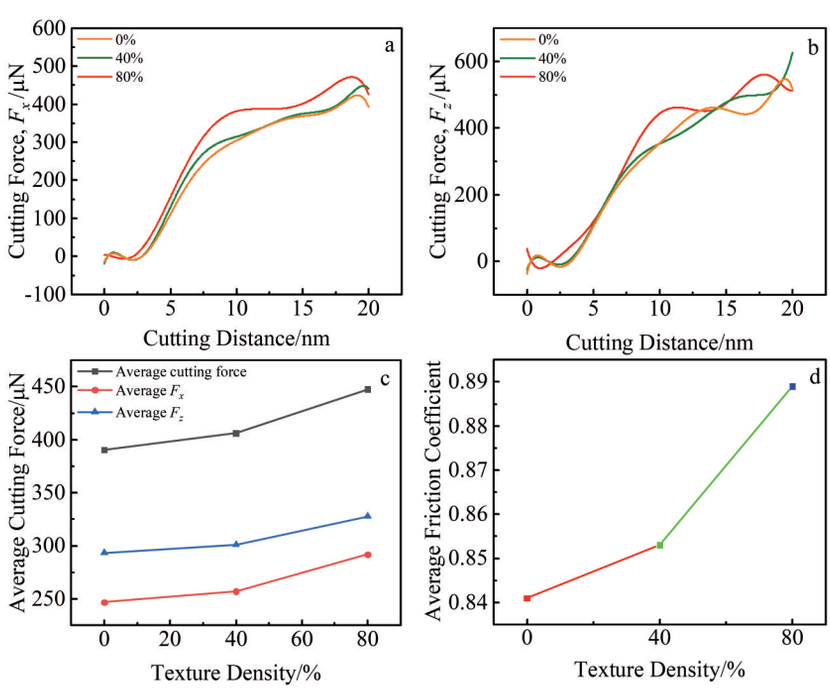

Fig.11 Cutting forces in extrusion mode along x direction (a) and z direction (b); average cutting forces (c) and average friction coefficients (d) at different texture densities

3 Conclusions

1) In shear cutting process of γ-TiAl, the rough surface can affect the formation of shear slip bands. With increasing the texture density, the number of stacking faults is increased, and the stacking faults are mainly formed on the chip. After the tool retraction, the workpiece surface with higher texture density becomes rough and shows the inferior subsurface quality.

2) In extrusion cutting process, the rough surface causes more and smaller stacking faults on the subsurface. However, the larger stacking faults occur on workpiece with higher texture density after tool retraction due to the influence of internal stress and tension. In addition, the extrusion can repair the surface cracks and internal cracks.

3) The regular rough surface can disturb chip and prevent burrs. During the cutting process, the rough surfaces near the tool path become smooth. However, during the tool retraction process, the texture around the tool becomes coarse and the large burr is generated.

4) The average friction coefficient and cutting force are mainly increased with increasing the texture density in both shear and extrusion modes. Only the radial cutting force shows a downward trend with increasing the texture density in shear mode.

References

1 Chae J, Park S S, Freiheit T. *International Journal of Machine Tools and Manufacture*[J], 2006, 46(3-4): 313
2 Qin Y, Brockett A, Ma Y *et al*. *The International Journal of Advanced Manufacturing Technology*[J], 2009, 47(9): 821
3 Kang Q, Fang X D, Sun L *et al*. *Computational Materials Science*[J], 2019, 170: 109 175
4 Zhang Quanli, Guo Nan, Chen Yan *et al. Micromachines*[J], 2019, 10(9): 573
5 Golshan A, Baharudin B T H T, Aoyama H *et al*. *Procedia Engineering*[J], 2017, 184: 192
6 Dève H E, Evens A G, Shih D S. *Acta Metallurgica et Materialia* [J], 1992, 40(6): 1259
7 Chen J H, Cao R. *Micromechanism of Cleavage Fracture of Metals*[M]. Oxford: Butterworth-Heinemann, 2015: 365
8 Priarone P C, Rizzuti S, Settineri L *et al*. *Journal of Materials Processing Technology*[J], 2012, 212(12): 2619
9 He L J, Su H H, Xu J H *et al*. *The International Journal of Advanced Manufacturing Technology*[J], 2017, 92(9): 4415
10 Wang Y D, Xu Z Y, Hu J C *et al*. *Materials Today Communications*[J], 2020, 25: 101 686
11 Silling S A, Lehoucq R. *Advances in Applied Mechanics*[J], 2010, 44: 73
12 Chamani M, Farrahi G H, Movahhedy M R. *Computational Materials Science*[J], 2016, 112: 175
13 Yasbolaghi R, Khoei A R. *Engineering Fracture Mechanics*[J], 2020, 226: 106 848
14 Kazanc S. *Physics Letters A*[J], 2007, 365(5-6): 473
15 Gissinger J R, Jensen B D, Wise K E. *Polymer*[J], 2017, 128: 211
16 Lazim R, Suh D, Choi S. *International Journal of Molecular Sciences*[J], 2020, 21(17): 6339
17 Dawson W, Gygi F. *The Journal of Chemical Physics*[J], 2018, 148(12): 124 501
18 Xiao G B, To S, Zhang G Q. *International Journal of Machine Tools and Manufacture*[J], 2021, 88: 214
19 Goel S, Martinez F D, Chavoshi S Z *et al*. *Journal of Micromanufacturing*[J], 2018, 1(1): 6
20 Li J, Fang Q H, Zhang L C *et al*. *Computational Materials Science*[J], 2015, 98: 252
21 Papanikolaou M, Salonitis K. *Applied Surface Science*[J], 2019, 467-468: 309
22 Feng R C, Song W Y, Li H Y *et al*. *Materials*[J], 2018, 11(6): 1025
23 Li J H, Feng R C, Qiao H Y *et al*. *Metals*[J], 2019, 9(12): 1278
24 Chubb S R, Papaconstantopoulos D A, Klein B M. *Physical Review B*[J], 1988, 38(17): 12 120
25 Tang F L, Cai H M, Bao H W *et al*. *Computational Materials Science*[J], 2014, 84: 232
26 Zope R R, Mishin Y. *Physical Review B*[J], 2003, 68(2): 24 102
27 Kim Y K, Kim H K, Jung W S *et al*. *Computational Materials Science*[J], 2016, 119: 1
28 Zhu Y, Zhang Y C, Qi S H *et al*. *Rare Metal Materials and Engineering*[J], 2016, 45(4): 897
29 Stukowski A. *Modelling and Simulation in Materials Science and Engineering*[J], 2009, 18(1): 15 012
30 Stukowski A, Bulatov V, Arsenlis A. *Modelling and Simulation in Materials Science and Engineering*[J], 2021, 20(8): 85 007
31 Wang J S, Fang F Z, Yan G P *et al*. *Nanomanufacturing and Metrology*[J], 2019, 2(3): 177

γ-TiAl加工过程中粗糙表面对材料去除和亚表面缺陷影响的分子动力学模拟

杨晟泽[1]，曹　卉[1,2]，刘　洋[1]，姚　鹏[1]，冯瑞成[1,2]

(1. 兰州理工大学 机电工程学院，甘肃 兰州 730050)

(2. 兰州理工大学 数字制造技术与应用教育部重点实验室，甘肃 兰州 730050)

摘　要：采用分子动力学方法模拟了γ-TiAl在纳米尺度下的加工响应。采用规则生成的粗糙工件表面，研究其对原子去除机理的影响。通过改变织构密度和刀具半径，研究了切削过程。结果表明，工件表面形貌对亚表面缺陷的产生和原子去除有不可忽视的影响，粗糙表面会影响剪切模式下切削过程中层错剪切带的形成。提高织构密度增加了亚表面缺陷的数量，加工表面的完整性因切割方式的不同而不同。刀具的相对锐度对切削机制和纹理效果有一定影响。

关键词：粗糙表面；材料去除；亚表面缺陷；分子动力学；γ-TiAl

作者简介：杨晟泽，男，1997年生，硕士生，兰州理工大学机电工程学院，甘肃 兰州 730050，电话：0931-5135199，E-mail：mikebraton@l63.com